

Expression of a CO₂-permeable aquaporin enhances mesophyll conductance in the C₄ species *Setaria viridis*

Maria Ermakova^{1*}, Hannah Osborn¹, Michael Groszmann¹, Soumi Bala¹, Samantha McGaughey¹, Caitlin Byrt¹, Hugo Alonso-Cantabrana¹, Steve Tyerman², Robert T. Furbank¹, Robert E. Sharwood^{1,3*}, Susanne von Caemmerer¹

¹ Australian Research Council Centre of Excellence for Translational Photosynthesis, Division of Plant Science, Research School of Biology, The Australian National University, Acton, Australian Capital Territory, 2601, Australia

² ARC Centre of Excellence in Plant Energy Biology, School of Agriculture Food and Wine, University of Adelaide, Glen Osmond, South Australia, 5064, Australia

³ Hawkesbury Institute for the Environment, Western Sydney University, Richmond, NSW, 2753, Australia

***Corresponding authors:** maria.ermakova@anu.edu.au and r.sharwood@westernsydney.edu.au

Key words: *Setaria viridis*, *Setaria italica*, aquaporin, CO₂ diffusion, mesophyll conductance, C₄ photosynthesis, C¹⁸O¹⁶O discrimination

Abstract

A fundamental limitation of photosynthetic carbon fixation is the availability of CO₂. In C₄ plants, primary carboxylation occurs in mesophyll cytosol, and little is known about the role of CO₂ diffusion in facilitating C₄ photosynthesis. We have examined the expression, localization, and functional role of selected plasma membrane intrinsic aquaporins (PIPs) from *Setaria italica* (foxtail millet) and discovered that *SiPIP2;7* is CO₂-permeable. When ectopically expressed in mesophyll cells of *S. viridis* (green foxtail), *SiPIP2;7* was localized to the plasma membrane and caused no marked changes in leaf biochemistry. Gas-exchange and C¹⁸O¹⁶O discrimination measurements revealed that targeted expression of *SiPIP2;7* enhanced the conductance to CO₂ diffusion from the intercellular airspace to the mesophyll cytosol. Our results demonstrate that mesophyll conductance limits C₄ photosynthesis at low *p*CO₂ and that *SiPIP2;7* is a functional CO₂ permeable aquaporin that can improve CO₂ diffusion at the airspace/mesophyll interface and enhance C₄ photosynthesis.

Diffusion of CO₂ across biological membranes is a fundamental aspect to photosynthesis. The significant contribution of aquaporins to increased CO₂ diffusion has been demonstrated in C₃ plants¹⁻³. Aquaporins have key roles in regulating the movement of water and solutes into roots and between tissues, cells and organelles⁴. These pore-forming integral membrane proteins can be divided into multiple sub-families depending on their amino acid sequence and sub-cellular localization. The PIPs (plasma membrane intrinsic proteins) are the only sub family, to date, known to permeate CO₂⁵. The PIPs are subdivided into paralog groups PIP1s and PIP2s, based on sequence homology⁶⁻⁸. Typically, PIP2s show higher water permeability when expressed in heterologous systems⁹ and PIP1s seemingly require interaction with a PIP2 to correctly traffic to the plasma membrane^{10,11}. In plants, a number of CO₂ permeable PIPs have been identified including *Arabidopsis thaliana* AtPIP1;2¹² and AtPIP2;1¹³; *Hordeum vulgare* HvPIP2;1, HvPIP2;2, HvPIP2;3 and HvPIP2;5¹⁴; *Nicotiana tabacum* NtPIP1;5s (NtAQP1)^{15,16} and *Zea mays* ZmPIP1;5 and ZmPIP1;6¹⁷.

The roles of the CO₂ permeable aquaporins have been largely characterized in C₃ photosynthetic plants where aquaporins localized in both the plasma membrane and chloroplast envelopes have been shown to facilitate CO₂ diffusion from the intercellular airspace to the site of Rubisco in chloroplasts^{18,19}. However, little is known about their role in C₄ photosynthesis. The C₄ photosynthetic pathway is a biochemical CO₂ pump where the initial conversion of CO₂ to bicarbonate (HCO₃⁻) by carbonic anhydrase (CA) and subsequent fixation to phosphoenolpyruvate (PEP) by PEP carboxylase (PEPC) takes

place in the cytosol of mesophyll cells. The pathway requires a close collaboration between mesophyll and bundle sheath cells and this constrains leaf anatomy limiting mesophyll surface area that forms a diffusive interface for CO₂²⁰. Mesophyll conductance is defined as the conductance to CO₂ diffusion from the intercellular airspace to the mesophyll cytosol²¹⁻²⁴. Although the rate of C₄ photosynthesis is almost saturated at ambient *p*CO₂, current modelling suggests that higher mesophyll conductance can increase assimilation rate and water-use-efficiency at low intercellular CO₂ partial pressures which occur when stomatal conductance is low²⁵.

Setaria italica (foxtail millet) and *Setaria viridis* (green foxtail) are C₄ grasses of the Paniceae tribe and Poaceae family, related to important agronomical crops such as *Z. mays* (maize) and *Sorghum bicolor* (sorghum). *S. viridis* is frequently used as a model species for C₄ photosynthesis research as it is diploid with a relatively small genome that is sequenced and can be easily transformed^{23,26,27}. Here we used a yeast heterologous expression system to examine the permeability to CO₂ of selected PIPs from *S. italica*. We identified *SiPIP2;7* as encoding a CO₂-permeable aquaporin that, when expressed in the plasma membrane of *S. viridis* mesophyll cells, increased mesophyll conductance. Our results demonstrate that CO₂-permeable aquaporins can be used to increase CO₂ diffusion from the intercellular airspace to mesophyll cytosol to provide higher carboxylation efficiency in C₄ leaves.

Results

S. italica PIP family

Four *PIP1* and eight *PIP2* genes were identified in both *S. italica* and *S. viridis* and their protein sequences were 99–100 % identical between the two species (Table S1). Phylogenetic analysis based on the amino acid sequences of the *S. italica* PIP family showed that three distinct clades emerge: the *PIP1* clade, *PIP2* clade I, and *PIP2* clade II (Fig. S1). Isoforms within these three clades have characteristic differences including sequence signatures associated with substrate selectivity (Table S2). Three of *SiPIP1*s (1;1, 1;2, 1;5) and all *SiPIP2* clade I members (2;1, 2;4, 2;5, 2;6, 2;7) matched the current consensus sequence for CO₂ transport^{6,28}.

RNA-seq data from the publicly available Phytomine database (Phytozome), was examined for tissue-specific expression patterns of the *S. italica* PIPs (Fig. 1a). *SiPIP1;1*, 1;2, 1;5, and 2;1 express at moderate to high levels and *SiPIP2;6* at low to moderate levels, in all tissues analyzed (root, leaves, shoot, panicle). *SiPIP1;6*, 2;4, 2;5, 2;7 and 2;3 were expressed predominantly in roots at low to moderate levels. *SiPIP2;8* was expressed only in leaves and *SiPIP2;2* transcripts were not detected.

Functional characterization of PIPs

GFP localization of SiPIP-GFP fusions were used to confirm expression and determine targeting to the yeast plasma membrane (Fig. 1b). Overall, SiPIP1s had lower GFP signal that was patchy at the cell periphery with strong internal signal consistent with localization to the endoplasmic reticulum. GFP signal was also present diffusively throughout the cytosol suggestive of protein degradation. Overall, SiPIP1s were poorly produced in yeast and were not efficiently targeting to the plasma membrane as needed for the functional assays. For the PIP2s, only SiPIP2;1, SiPIP2;4, SiPIP2;5, and SiPIP2;7 showed clear localization to the plasma membrane in addition to other internal structures, and were therefore selected for further functional analyses.

CO₂ permeability was measured in yeast co-expressing a *SiPIP* along with *human CARBONIC ANHYDRASE II (hCAII)*. A stopped flow spectrophotometer was used to monitor CO₂-triggered intracellular acidification via changes in fluorescence intensity of a pH sensitive fluorescein dye Fig. S2; ^{12,18,29}. Importantly for reliable results, all SiPIP yeast lines tested showed similar cell volumes and were not limited by CA activity (Fig. S2). A screen of the lines revealed that yeast expressing *SiPIP2;7* had the highest CO₂ permeability of $1.5 \times 10^{-4} \text{ m s}^{-1}$, which was significantly larger than the negative control expressing *hCAII* only (Fig. 1c). Other *SiPIPs* displayed comparable CO₂ permeability to the *hCAII* only control. The changes in CO₂ permeability detected on the stopped flow spectrophotometer for yeast expressing *SiPIP2;7* were not an artifact brought on by an increased permeability to protons causing the intracellular acidification (Fig. S3).

Freeze-thaw survival assays, which quantify water permeability of aquaporins ³⁰, provided further confirmation that the SiPIPs expressed in yeast were functional. Overexpression of water permeable aquaporins greatly improves freeze-thaw tolerance in yeast, especially in the highly compromised aquaporin knockout mutant *aqy1/2* ³⁰. Yeast expressing the β -glucuronidase reporter gene (515.GUS) was used a control to show that the single freeze-thaw treatment was effective in almost killing off the entire yeast population (Fig. 1d). Consistent with the poor plasma membrane localization and abundance of SiPIP2;1-GFP (Fig. 1b), yeast expressing *SiPIP2;1* did not show any protection to freeze-thaw treatments (Fig. 1c). On the other hand, *SiPIP2;4*, *2;5* and *2;7* all showed some level of protection, indicating that they permeated water and were functional within the plasma membrane of yeast cells. For detailed characterisation of water permeability, SiPIP2;7 was expressed in *Xenopus laevis* oocytes. Swelling assay confirmed that SiPIP2;7 is a functional water channel (Fig. S4).

Expression of PIP2;7 in mesophyll cells of *S. viridis*

To confirm and exploit the CO₂ permeability characteristic of SiPIP2;7 *in planta*, we created transgenic *S. viridis* plants expressing *SiPIP2;7* with a C-terminal FLAG-tag fusion and under the control of the mesophyll-preferential *Z. mays* PEPC promoter^{31,32}. Out of 52 T₀ plants analyzed for SiPIP2;7-FLAG protein abundance and the hygromycin phosphotransferase (*hpt*) gene copy number (Fig. S5), lines 27, 44 and 52 were selected for further analysis because they had the strongest FLAG signal per transgene insertion number. Immunodetection of FLAG and photosynthetic proteins was performed on leaves of homozygous transgenic plants (Fig. 2a); azygous plants of line 44 were used as control hereafter. Monomeric and dimeric SiPIP2;7-FLAG was detected in all transgenic plants (Fig. S5) and abundance of the prevalent dimeric form was used for relative quantification of SiPIP2;7 abundance (Fig. 2a). Plants of line 44 had the highest production of SiPIP2;7-FLAG whilst plants of lines 27 and 52 accumulated about 2-4 times less of this protein. Immunodetection of FLAG on leaf cross-sections, visualized with confocal microscopy, confirmed partial localization of SiPIP2;7-FLAG to the plasma membrane of mesophyll cells (Fig. 2c). Transcript analysis confirmed highly elevated expression of *SiPIP2;7-FLAG* in leaves, but not in roots of transgenic lines (Fig. S6).

Abundances of photosynthetic proteins PEPC, CA, the Rieske subunit of the Cytochrome *b₆f* complex, and the small subunit of Rubisco (RbcS), did not differ between transgenic and control plants (Fig. 2a). In line with the immunoblotting results, measured activities of PEPC and CA, and the amount of Rubisco active sites were not altered in the transgenic plants (Table 1). Chlorophyll content, leaf dry weight per area and biomass of roots and shoots did not differ between the genotypes either (Table 1).

To study the effects of *SiPIP2;7-FLAG* ectopic expression on photosynthetic properties in the transgenic plants, we conducted concurrent gas-exchange and fluorescence analyses at different intercellular CO₂ partial pressure (*C_i*) (Fig. 3). No significant changes were detected between transgenic and control plants in CO₂ assimilation rates (*A*), effective quantum yield of Photosystem II (ϕ PSII) or stomatal conductance to water vapor at ambient CO₂ (Fig. S7). However, since CO₂ assimilation rates were consistently higher in all transgenic plants at low *C_i* (Fig. 3a, inset), we analyzed the initial slopes of the CO₂ response curves and mesophyll conductance. Fitting linear regressions (Fig. 4a) indicated that lines 44 and 52 had significantly greater initial slopes (average values of 0.52 and 0.53, respectively) compared to the control (0.41), whereas line 27 had a slightly increased initial slope (0.46).

137 Mesophyll conductance to CO₂ in plants expressing SiPIP2;7

Measurements of $\Delta^{18}\text{O}$ were used to estimate conductance of CO_2 from the intercellular airspace to the sites of CO_2 and H_2O exchange in the mesophyll cytosol (g_m) with the assumption that CO_2 was in full isotopic equilibrium with leaf water in the cytosol^{23,33}. Transgenic lines 27 and 44 had significantly greater mesophyll conductance than control plants ($0.42 \text{ mol m}^{-2} \text{ s}^{-1} \text{ bar}^{-1}$) with average values of 0.59 and $0.55 \text{ mol m}^{-2} \text{ s}^{-1} \text{ bar}^{-1}$, respectively (Fig. 4b). We also used the g_m calculations proposed by Ogée *et al.*³⁴ which try to account for the rates of bicarbonate consumption by CA. The CA hydration constant (k_{CA}) of $6.5 \text{ mol m}^{-2} \text{ s}^{-1} \text{ bar}^{-1}$ was used for these calculations (Table 1). We found that the g_m measured with this method gave on average 1.25 times greater values but did not change the ranking of mesophyll conductance shown in Fig. 4a (Fig. S8). The C_4 photosynthetic model by von Caemmerer and Furbank³⁵ and von Caemmerer³⁶ relates the initial slope of the CO_2 response curve (dA/C_i) to g_m (see Fig. 4 caption and Materials and Methods). Fig. 4c shows that the measured relationship between the initial slope and g_m fits closely with model prediction.

Discussion

The diffusion of CO_2 from the earth's atmosphere to the site of primary carboxylation within leaves of C_3 and C_4 plants often limits photosynthesis and impacts the efficient use of water. In C_4 plants, primary carboxylation occurs in mesophyll cytosol and a large mesophyll conductance, g_m , is required to account for high photosynthetic rates which generate a large drawdown between the intercellular airspace and the cytosol²¹. An effective strategy to enhance CO_2 diffusion in C_3 plants has been the overexpression of CO_2 permeable aquaporins in plasma membrane and the chloroplast envelope leading to improved g_m , assimilation rate or grain yield^{1,3,15,37}. Screening *S. italica* PIPs for CO_2 permeability in a yeast heterologous system resulted in identification of SiPIP2;7 as a CO_2 pore (Fig. 1c). Expression analysis revealed that *SiPIP2;7* was almost exclusively expressed in roots under ideal conditions (Fig. 1a, Fig. S6) which, combined with the water permeability identified in yeast and oocyte assays (Fig. 1d, Fig. S4), suggest that SiPIP2;7 may function in regulating root hydraulic conductivity, a role extensively documented for PIP aquaporins^{38,39}. The physiological relevance of SiPIP2;7's CO_2 permeating capacity is not immediately clear. Gas uptake by roots is well documented⁴⁰ and in C_3 plants CO_2 uptake by roots may contribute to the C_4 photosynthesis-like metabolism detected in stems and petioles⁴¹. It is possible that *SiPIP2;7* is conditionally expressed in leaves, or even that its capacity to transport CO_2 is inadvertent and related to the transportation of another yet undetermined substrate; analogous to the uptake of toxic metalloids by some NIP aquaporins due to their capacity to

168 transport boron⁴². Further work is needed to determine whether PIPs in general function natively as
169 relevant CO₂ pores in C₄ leaves.

170 We employed the CO₂ transport capacity of SiPIP2;7 to enhance transmembrane CO₂ diffusion from
171 the intercellular airspace into the mesophyll cytosol, where CA and PEPC reside, by overexpressing
172 *SiPIP2;7* in *S. viridis*. We confirmed the localization of SiPIP2;7 within the mesophyll plasma membranes
173 (Fig. 2c) and detected the increase in CO₂ diffusion across the mesophyll membranes in transgenic
174 plants by two independent methods. First, we calculated g_m from the C¹⁸O¹⁶O discrimination
175 measurements (Fig. 4b) and the theory for these calculations has been outlined^{23,33,43}. Second, we
176 fitted linear regressions to the initial slopes of the A_{Ci} curves (Fig. 3a inset, Fig. 4a), which depend on
177 g_m , V_{pmax} and K_p where the two latter parameters denote the maximum PEPC activity and the Michaelis
178 Menten constant of PEPC for HCO₃⁻^{35,36}. Since PEPC and CA activities were not altered in plants
179 expressing *SiPIP2;7* (Table 1), higher initial slopes of the A_{Ci} curves in transgenic lines were attributed
180 to the increased g_m . Up-regulation of g_m in lines 27 and 52 was confirmed by one of the methods, while
181 both methods indicated significantly increased g_m in line 44 (Fig. 4). When plotted against each other,
182 the initial slopes and g_m in transgenic and control plants, fitted the model predictions confirming the
183 hypothesised functional role of g_m in C₄ photosynthesis^{24,36,44}. Our findings explicitly demonstrate that
184 mesophyll conductance limits C₄ photosynthesis at low CO₂ and indicate that increasing CO₂ diffusion
185 at the airspace/mesophyll interface, combined with complementary traits including overexpression of
186 Cytochrome *b₆f* and Rubisco^{27,31}, could further improve C₄ photosynthesis.

187 **Materials and methods**

188 **Heterologous expression in yeast**

189 cDNAs encoding the 12 *S. italica* aquaporins (Table S1) and *human CARBONIC ANHYDRASE II*
190 (AK312978) were codon-optimized for expression in yeast with IDT DNA tool
191 (<https://sg.idtdna.com/pages/tools>) and a yeast related kozak sequence was added at the 5' end to
192 help increase translation⁴⁵. For CO₂ permeability measurements, pSF-TPI1-URA3 with an aquaporin
193 and pSF-TEF1-LEU2 with hCAII were co-transformed into the *S. cerevisiae* strain INVSc1 (Thermo Fisher
194 Scientific, Waltham, MA). For water permeability measurements, pSF-TPI1-URA3 with an aquaporin
195 was transformed into the *aqy1/2* double mutant yeast strain deficient in aquaporins⁴⁶. The yeast
196 vectors pSF-TPI1-URA3 and pSF-TEF1-LEU2 were obtained from Oxford Genetics (Oxford, UK). Yeast
197 transformation was performed using the Frozen-EZ yeast transformation II kit (Zymo Research, Irvine,
198 CA) and selection of positive transformants was based on amino acid complementation. To ensure CA

was not limiting, CA activity was determined using a membrane inlet mass spectrometry as described by Endeward, et al.⁴⁷ (Fig. S2). For CO₂ permeability measurements an average cell diameter of 4.63 µm was determined by measuring ~100 yeast cells expressing each aquaporin (Fig. S2). To study the subcellular localizations of aquaporins in yeast, a C-terminus GFP tag was added to the sequences into the pSF-TPI1-URA3 vector (pSF-TPI1-URA3-GFP). The fluorescence signal was observed using a Zeiss 780 confocal laser scanning microscope (Zeiss, Oberkochen, Germany): excitation 488 nm, emission 530 nm. Cytosolic GFP expression was used as control.

CO₂ induced intracellular acidification assay

CO₂ intracellular acidification was measured in yeast cells loaded with fluorescein diacetate (Sigma-Aldrich, St. Louis, MO) as described previously^{48,49}. Briefly, an overnight culture of yeast cells was collected and resuspended in an equal volume of 50 mM 4-(2-hydroxyethyl)-1-piperazineethanesulfonic acid (HEPES)-NaOH, pH 7.0, 50 µM fluorescein diacetate and incubated for 30 min in the dark at 37 °C. The suspension was centrifuged and the pellet resuspended in ice-cold incubation buffer (25 mM HEPES-NaOH, pH 6.0, 75 mM NaCl). Cells loaded with fluorescein diacetate were then injected into the stopped flow spectrophotometer (DX.17MV; Applied Photophysics, Leatherhead, UK) alongside a buffer solution (25 mM HEPES, pH 6.0, 75 mM NaHCO₃, bubbled with CO₂ for 2 h). The kinetics of acidification was measured at 490 nm excitation and >515 nm emission (OG515 long pass filter, Schott, supplied by Applied Photophysics). Data was collected over a time interval of 0.2 s and analysed using ProData SX viewer software (Applied Photophysics). CO₂ permeability was determined using the method of Yang, et al.⁵⁰. An average of 75 injections over at least three separate cultures was used for each aquaporin.

Determination of water permeability

A freeze-thaw yeast assay was used to determine water permeability of aquaporins expressed in *aqy1/2* based on previous reports³⁰. Briefly, an overnight culture was diluted to ~6x10⁶ cells (final volume 1 mL) in appropriate selection liquid growth medium and incubated at 30°C for 1 h. 250 µL of each culture were then aliquoted into two standard 1.5 mL microtubes: the first (control) tube was placed on ice and the second tube was subject to a single freeze-thaw treatment, consisting of 30-s freezing in liquid nitrogen and thawing for 20 min in a 30 °C water bath. Following the treatment, the cells were placed on ice. The tubes were then vortexed briefly to ensure even suspension of cells and 200 µL of the culture was transferred to wells of a Nunc-96 400 µL flat bottom untreated plate (Thermo Fisher Scientific, Cat#243656). Yeast growth in control and treated cultures were monitored over a 24-

230 30 h period in a M1000 Pro plate reader (TECAN, Männedorf, Switzerland) at 30 °C with double orbital
231 shaking at 400 rpm and measuring absorbance at 650 nm every 10 min. Growth data was log
232 transformed and freeze-thaw survival calculated as the growth (area under the curve) of treated
233 culture relative to its untreated control from time zero up until the untreated control culture reached
234 stationary phase.

235 For swelling assays, the coding sequence of *SiPIP2;7* was cloned into pGEMHE oocyte expression vector
236 using LR clonase II (Thermo Fisher Scientific) and cRNA was synthesised with mMessage mMachine®
237 T7 Transcription Kit (Thermo Fisher Scientific). *Xenopus laevis* oocytes were injected with 46 nL of
238 RNase-free water with either no cRNA or 23 ng cRNA with a micro-injector Nanoinject II (Drummond
239 Scientific, Broomall, PA). Post-injection oocytes were stored at 18°C in a Low Na⁺ Ringer's solution [62
240 mM NaCl, 36 mM KCl, 5 mM MgCl₂, 0.6 mM CaCl₂, 5 mM HEPES, 5% (v/v) horse serum (H-1270, Sigma-
241 Aldrich) and antibiotics: 0.05 mg mL⁻¹ tetracycline, 100 units mL⁻¹ penicillin/0.1 mg mL⁻¹ streptomycin],
242 pH 7.6 for 24–30 h. Photometric swelling assay was performed 24-30 h post-injection ⁵¹.

243 **Construct assembly and *S. viridis* transformation**

244 The coding sequence of *S. viridis* *PIP2;7* (Sevir.2G128300.1, Phytozome,
245 <https://phytozome.jgi.doe.gov/>) has been codon optimized for the Golden Gate cloning ⁵² and
246 translationally fused with the glycine linker and the FLAG-tag coding sequence ⁵³. The resulting coding
247 sequence was assembled with the *Z. mays* *PEPC* promoter and the bacterial tNos terminator into the
248 second expression module of the pAGM4723 binary vector. The first expression module has been
249 occupied by the hygromycin phosphotransferase (*hpt*) gene assembled with the *Oryza sativa* actin
250 promoter and the tNos terminator. The construct was transformed into *S. viridis* cv. MEO V34-1 using
251 *Agrobacterium tumefaciens* strain AGL1 following the procedure described in Osborn, et al. ²³. T₀ plants
252 resistant to hygromycin were transferred to soil and analyzed for *hpt* insertion number by droplet
253 digital PCR (iDNA Genetics, Norwich, UK). The T₁ and T₂ progenies of T₀ plants 27, 44 and 52 were
254 analyzed. Azygous T₁ plants of line 44 and their progeny were used as control.

255 **Plant growth conditions**

256 Seeds were surface-sterilized and germinated on medium (pH 5.7) containing 2.15 g L⁻¹ Murashige and
257 Skoog salts, 10 mL L⁻¹ 100x Murashige and Skoog vitamins stock, 30 g L⁻¹ sucrose, 7 g L⁻¹ Phytoblend,
258 20 mg L⁻¹ hygromycin (no hygromycin for azygous plants). Seedlings that developed secondary roots
259 were transferred to 0.6 L pots with garden soil mix layered on top with 2 cm seed raising mix (Debco,

260 Tyabb, Australia) both containing 1 g L⁻¹ Osmocote (Scotts, Bella Vista, Australia). Plants were grown in
261 controlled environmental chambers with 16 h light/8 h dark, 28 °C day, 22 °C night, 60% humidity and
262 ambient CO₂ concentrations. Light intensity of 300 μmol m⁻² s⁻¹ was supplied by 1000 W red sunrise
263 3200 K lamps (Sunmaster Growlamps, Solon, OH). Youngest fully expanded leaves of the 3–4 weeks
264 plants before flowering were used for all analyses.

265 **Chlorophyll and enzyme activity**

266 Chlorophyll content was measured on frozen leaf discs homogenised with a TissueLyser II (Qiagen,
267 Venlo, The Netherlands)⁵⁴. PEPC activity was determined after Pengelly, et al.⁵⁵ from fresh leaf extracts
268 from the plants adapted for 1 h to 800 μmol photons m⁻² s⁻¹. CA activity was measured on a membrane
269 inlet mass spectrometer as a rate of ¹⁸O exchange from labelled ¹³C¹⁸O₂ to H₂¹⁶O at 25 °C according to
270 von Caemmerer, et al.⁵⁶ by calculating the hydration rate after Jenkins, et al.⁵⁷. The amount of Rubisco
271 active sites was determined by [¹⁴C] carboxyarabinitol biphosphate binding as described earlier⁵⁸.

272 **RNA isolation and qPCR**

273 Leaf and root tissue were frozen in liquid N₂. Leaf samples were homogenised using a TissueLyser II
274 and RNA was extracted using the RNeasy Plant Mini Kit (Qiagen). Roots were ground with mortar and
275 pestle in liquid N₂ and RNA was isolated according to Massey⁵⁹. Briefly, 150 μL of pre-heated (60 °C)
276 extraction buffer [0.1 M trisaminomethane (Tris)-HCl, pH 8, 5 mM ethylenediaminetetraacetic acid
277 (EDTA), 0.1 M NaCl, 0.5% sodium dodecyl sulfate (SDS), 1% 2-mercaptoethanol) was added to ~100 mg
278 of fine root powder and incubated at 60 °C for 5 min. 150 μL of phenol:chloroform:isoamyl alcohol
279 (25:24:1) saturated with 10 mM Tris (pH 8.0) and 1 mM EDTA was added to the samples, vortexed
280 vigorously for 10 min and centrifuged at 4500 g for 15 min. Aqueous phase was mixed with 120 μL of
281 isopropanol and 15 μL of 3 M sodium acetate and incubated at -80 °C for 15 min, then centrifuged at
282 4500 g (30 min, 4 °C). The pellet was washed twice in 300 μL of ice-cold 70% ethanol, air dried and
283 dissolved in 60 μL of RNase-free water. After addition of 40 μL of 8 M LiCl, samples were incubated
284 overnight at 4 °C. Nucleic acids were pelleted by centrifugation at 16,000 g (60 min, 4 °C), washed twice
285 with 200 μL of ice-cold 70% ethanol, air dried and dissolved in RNase-free water. DNA from the samples
286 was removed using an Ambion TURBO DNA free kit (Thermo Fisher Scientific), and RNA quality was
287 determined using a NanoDrop (Thermo Fisher Scientific). 100 ng of total RNA were reverse transcribed
288 into cDNA using a SuperScript™ III Reverse Transcriptase (Thermo Fisher Scientific). qPCR and melt
289 curve analysis were performed on a Viia7 Real-time PCR system (Thermo Fisher Scientific) using the
290 Power SYBR green PCR Master Mix (Thermo Fisher Scientific) according to the manufacturer's protocol.

291 Primer pairs designed to distinguish between *S. viridis* *PIP2;6* and *PIP2;7* using Primer3 in Geneious
292 Prime (<https://www.geneious.com>) and reference primers are listed in Table S3.

293 **Western blotting and immunolocalization**

294 Protein isolation from leaves and gel electrophoresis were performed as described earlier ²⁷. Proteins
295 were probed with antibodies against FLAG (ab49763, 1:5000, Abcam, Cambridge, UK), RbcS ⁶⁰
296 (1:10,000), Rieske (AS08 330, 1:3000, Agrisera, Vännäs Sweden), PEPC (AS09 458, 1:10,000, Agrisera),
297 CA ⁶¹ (1:10,000). Quantification of immunoblots was performed with Image Lab software (Biorad,
298 Hercules, CA). For immunolocalization leaf tissue was fixed and probed with primary antibodies against
299 FLAG (1:40) and secondary goat anti-mouse Alexa Fluor 488-conjugated antibodies (ab150113, 1:200,
300 Abcam) as described in Ermakova, et al. ⁶². Images were captured with a Zeiss 780 microscope using
301 ZEN 2012 software (Black edition, Zeiss, Oberkochen, Germany). Images for plants of lines 27, 44 and
302 azygous plants were acquired using online fingerprinting (488 nm excitation) with three user-defined
303 spectral profiles for AlexaFluor488, endogenous autofluorescence and chlorophyll. The spectral profile
304 for endogenous autofluorescence was derived from the azygous control. The image for line 52 was
305 initially collected as a full spectral scan (490-660 nm), then linearly un-mixed using the same online
306 fingerprint settings as previously described. Images were post-processed with FIJI ⁶³, and histograms
307 for all images were min-max adjusted.

308 **Gas exchange measurements**

309 Gas-exchange and fluorescence analysis were performed at an irradiance of 1500 $\mu\text{mol m}^{-2} \text{s}^{-1}$ (90%
310 red/10% blue actinic light) and different intercellular CO_2 partial pressures using a LI-6800 (LI-COR
311 Biosciences, Lincoln, NE) equipped with a fluorometer head 6800-01 A (LI-COR Biosciences). Leaves
312 were first equilibrated at 400 ppm CO_2 in the reference side, leaf temperature 25 °C, 60% humidity and
313 flow rate 500 $\mu\text{mol s}^{-1}$ and then a stepwise increase of CO_2 concentrations from 0 to 1600 ppm was
314 imposed at 3 min intervals. Initial slopes of the CO_2 response curves were determined by linear fitting
315 in OriginPro 2018b (OriginLab, Northampton, MA). Quantum yield of PSII upon the application of
316 multiphase saturating pulses (8000 $\mu\text{mol m}^{-2} \text{s}^{-1}$) was calculated according to Genty, et al. ⁶⁴.

317 **$\text{C}^{18}\text{O}^{16}\text{O}$ discrimination measurements**

318 Simultaneous measurements of exchange of CO_2 , H_2O , $\text{C}^{18}\text{O}^{16}\text{O}$ and H_2^{18}O were made by coupling two
319 LI-6400XT gas-exchange systems to a tunable diode laser (TDL: model TGA200A, Campbell Scientific
320 Inc., Logan, UT) to measure $\text{C}^{18}\text{O}^{16}\text{O}$ discrimination and a Cavity Ring-Down Spectrometer (L2130-i,

Picarro Inc., Sunnyvale, CA) to measure the oxygen isotope composition of water vapor ²³. Measurements were made at 2% O₂, 380 μmol mol⁻¹ CO₂, leaf temperature of 25 °C, irradiance of 1500 μmol m⁻² s⁻¹ and relative humidity of 55%. Each leaf was measured at 4 min intervals and 10 readings were taken. Mesophyll conductance was calculated as described by Osborn, et al. ²³ with the assumptions that there was sufficient carbonic anhydrase (CA) in the mesophyll cytosol for isotopic equilibration between CO₂ and HCO₃⁻. We also used the calculations proposed by Ogée, et al. ³⁴ to estimate *g_m*. These calculations try to account for the rates of bicarbonate consumption by CA. We used the rate constant of CA hydration (*k_{CA}*) of 6.5 mol m⁻² s⁻¹ bar⁻¹ for these calculations.

Statistical analysis

One-way ANOVAs with Tukey post-hoc test were performed in OriginPro 2018b. A two-tailed, heteroscedastic Student's *t*-tests were performed in Microsoft Excel.

Data availability

The datasets and materials generated during the current study are available from the corresponding authors on request.

The authors declare no competing interests

Acknowledgements and funding sources

We thank Xueqin Wang for *S. viridis* transformation, Zac Taylor for gas-exchange measurements, Murray Badger and Dimitri Tolleter for measuring CA activity in yeast, Daryl Webb, Ayla Manwaring and the Centre for Advanced Microscopy at the Australian National University for confocal imaging, Wendy Sullivan for help with the stopped flow spectrophotometry and Nerea Ubierna for sharing her spreadsheet for the Ogée *et al.* *g_m* calculations. Funding information: this research was supported by the Australian Research Council (ARC) Centre of Excellence for Translational Photosynthesis (CE140100015). RES was funded by ARC DECRA (DE130101760). This work is presented in the Australian provisional patent application # 2021900409.

Author contributions: RES, SVC, RTF and ME designed the research. ME, HO, MG, SB, SM, RES and SVC performed experiments. ME, RES, SVC and HO wrote the manuscript with contribution of MG. All authors contributed to data analysis and manuscript editing.

References

- Flexas, J. *et al.* Tobacco aquaporin NtAQP1 is involved in mesophyll conductance to CO₂ in vivo. *The Plant Journal* **48**, 427-439, doi:10.1111/j.1365-3113.2006.02879.x (2006).
- Sade, N. *et al.* The Role of Tobacco Aquaporin1 in Improving Water Use Efficiency, Hydraulic Conductivity, and Yield Production Under Salt Stress. *Plant Physiology* **152**, 245, doi:10.1104/pp.109.145854 (2010).
- Hanba, Y. T. *et al.* Overexpression of the Barley Aquaporin HvPIP2;1 Increases Internal CO₂ Conductance and CO₂ Assimilation in the Leaves of Transgenic Rice Plants. *Plant and Cell Physiology* **45**, 521-529, doi:10.1093/pcp/pch070 (2004).
- Tyerman, S. D., McGaughey, S. A., Qiu, J., Yool, A. J. & Byrt, C. S. Adaptable and multifunctional ion-conducting aquaporins. *Annual Review of Plant Biology* **72**, doi:10.1146/annurev-arplant-081720-013608 (2021).
- Uehlein, N., Kai, L. & Kaldenhoff, R. in *Plant Aquaporins: From Transport to Signaling* (eds François Chaumont & Stephen D. Tyerman) 255-265 (Springer International Publishing, 2017).
- Azad, A. K. *et al.* Genome-Wide Characterization of Major Intrinsic Proteins in Four Grass Plants and Their Non-Aqua Transport Selectivity Profiles with Comparative Perspective. *PLOS ONE* **11**, e0157735, doi:10.1371/journal.pone.0157735 (2016).
- Chaumont, F., Barrieu, F., Wojcik, E., Chrispeels, M. J. & Jung, R. Aquaporins Constitute a Large and Highly Divergent Protein Family in Maize. *Plant Physiology* **125**, 1206, doi:10.1104/pp.125.3.1206 (2001).
- Groszmann, M., Osborn, H. L. & Evans, J. R. Carbon dioxide and water transport through plant aquaporins. *Plant, Cell & Environment* **40**, 938-961, doi:<https://doi.org/10.1111/pce.12844> (2017).
- Chaumont, F., Barrieu, F., Jung, R. & Chrispeels, M. J. Plasma Membrane Intrinsic Proteins from Maize Cluster in Two Sequence Subgroups with Differential Aquaporin Activity. *Plant Physiology* **122**, 1025, doi:10.1104/pp.122.4.1025 (2000).
- Berny, Marie C., Gilis, D., Rooman, M. & Chaumont, F. Single Mutations in the Transmembrane Domains of Maize Plasma Membrane Aquaporins Affect the Activity of Monomers within a Heterotetramer. *Molecular Plant* **9**, 986-1003, doi:<https://doi.org/10.1016/j.molp.2016.04.006> (2016).
- Zelazny, E. *et al.* FRET imaging in living maize cells reveals that plasma membrane aquaporins interact to regulate their subcellular localization. *Proceedings of the National Academy of Sciences* **104**, 12359, doi:10.1073/pnas.0701180104 (2007).
- Heckwolf, M., Pater, D., Hanson, D. T. & Kaldenhoff, R. The Arabidopsis thaliana aquaporin AtPIP1;2 is a physiologically relevant CO₂ transport facilitator. *Plant Journal* **67**, 795-804 (2011).
- Wang, C. *et al.* Reconstitution of CO₂ Regulation of SLAC1 Anion Channel and Function of CO₂-Permeable PIP2;1 Aquaporin as CARBONIC ANHYDRASE4 Interactor. *The Plant Cell* **28**, 568-582, doi:10.1105/tpc.15.00637 (2016).
- Mori, I. C. *et al.* CO₂ Transport by PIP2 Aquaporins of Barley. *Plant and Cell Physiology* **55**, 251-257, doi:10.1093/pcp/pcu003 (2014).
- Uehlein, N., Lovisolo, C., Siefritz, F. & Kaldenhoff, R. The tobacco aquaporin NtAQP1 is a membrane CO₂ pore with physiological functions. *Nature* **425**, 734-737, doi:10.1038/nature02027 (2003).
- De Rosa, A., Watson-Lazowski, A., Evans, J. R. & Groszmann, M. Genome-wide identification and characterisation of Aquaporins in Nicotiana tabacum and their relationships with other Solanaceae species. *BMC Plant Biology* **20**, 266, doi:10.1186/s12870-020-02412-5 (2020).
- Heinen, R. B. *et al.* Expression and characterization of plasma membrane aquaporins in stomatal complexes of Zea mays. *Plant Molecular Biology* **86**, 335-350, doi:10.1007/s11103-014-0232-7 (2014).
- Uehlein, N. *et al.* Function of Nicotiana tabacum aquaporins as chloroplast gas pores challenges the concept of membrane CO₂ permeability. *The Plant cell* **20**, 648-657, doi:10.1105/tpc.107.054023 (2008).
- Kaldenhoff, R. Mechanisms underlying CO₂ diffusion in leaves. *Current Opinion in Plant Biology* **15**, 276-281, doi:<http://dx.doi.org/10.1016/j.pbi.2012.01.011> (2012).
- von Caemmerer, S., Evans, J., Cousins, A., Badger, M. & Furbank, R. Charting new pathways to C₄ rice. (2007).

- 21 Evans, J. R. & von Caemmerer, S. Carbon dioxide diffusion inside leaves. *Plant Physiology* **110**, 339-346 (1996).
- 22 Barbour, M. M., Evans, J. R., Simonin, K. A. & von Caemmerer, S. Online CO₂ and H₂O oxygen isotope fractionation allows estimation of mesophyll conductance in C₄ plants, and reveals that mesophyll conductance decreases as leaves age in both C₄ and C₃ plants. *New Phytologist* **210**, 875-889, doi:10.1111/nph.13830 (2016).
- 23 Osborn, H. L. *et al.* Effects of reduced carbonic anhydrase activity on CO₂ assimilation rates in *Setaria viridis*: a transgenic analysis. *Journal of Experimental Botany* **68**, 299-310, doi:10.1093/jxb/erw357 (2016).
- 24 Ubierna, N., Gandin, A., Boyd, R. A. & Cousins, A. B. Temperature response of mesophyll conductance in three C₄ species calculated with two methods: ¹⁸O discrimination and in vitro V_{pmax}. *New Phytologist* **214**, 66-80, doi:10.1111/nph.14359 (2017).
- 25 von Caemmerer, S. & Furbank, R. T. Strategies for improving C₄ photosynthesis. *Current Opinion in Plant Biology* **31**, 125-134, doi:<http://dx.doi.org/10.1016/j.pbi.2016.04.003> (2016).
- 26 Brutnell, T. P. *et al.* *Setaria viridis*: a model for C₄ photosynthesis. *The Plant Cell Online* **22**, 2537-2544 (2010).
- 27 Ermakova, M., Lopez-Calcano, P. E., Raines, C. A., Furbank, R. T. & von Caemmerer, S. Overexpression of the Rieske FeS protein of the Cytochrome b₆f complex increases C₄ photosynthesis in *Setaria viridis*. *Communications Biology* **2**, doi:<https://doi.org/10.1038/s42003-019-0561-9> (2019).
- 28 Perez Di Giorgio, J. *et al.* Prediction of Aquaporin Function by Integrating Evolutionary and Functional Analyses. *The Journal of Membrane Biology* **247**, 107-125, doi:10.1007/s00232-013-9618-8 (2014).
- 29 Ding, X. *et al.* Water and CO₂ permeability of SsAqpZ, the cyanobacterium *Synechococcus* sp. PCC7942 aquaporin. *Biology of the Cell* **105**, 118-128, doi:<https://doi.org/10.1111/boc.201200057> (2013).
- 30 Tanghe, A. *et al.* Aquaporin expression correlates with freeze tolerance in baker's yeast, and overexpression improves freeze tolerance in industrial strains. *Appl Environ Microbiol* **68**, 5981-5989, doi:10.1128/aem.68.12.5981-5989.2002 (2002).
- 31 Salesse-Smith, C. E. *et al.* Overexpression of Rubisco subunits with RAF1 increases Rubisco content in maize. *Nature Plants* **4**, 802-810, doi:10.1038/s41477-018-0252-4 (2018).
- 32 Gupta, S. D. *et al.* The C₄Ppc promoters of many C₄ grass species share a common regulatory mechanism for gene expression in the mesophyll cell. *The Plant Journal* **101**, 204-216, doi:10.1111/tjp.14532 (2020).
- 33 Barbour, M. M., Evans, J. R., Simonin, K. A. & von Caemmerer, S. Online CO₂ and H₂O oxygen isotope fractionation allows estimation of mesophyll conductance in C₄ plants, and reveals that mesophyll conductance decreases as leaves age in both C₄ and C₃ plants. *New Phytologist* **210**, 875-889 doi:10.1111/nph.13830 (2016).
- 34 Ogée, J., Wingate, L. & Genty, B. Estimating Mesophyll Conductance from Measurements of C₃ and C₄ Photosynthetic Discrimination and Carbonic Anhydrase Activity. *Plant Physiology* **178**, 728, doi:10.1104/pp.17.01031 (2018).
- 35 von Caemmerer, S. & Furbank, R. T. in *The biology of C₄ Photosynthesis* (eds Rowan F. Sage & Russell K. Monson) 173-211 (Academic Press, 1999).
- 36 von Caemmerer, S. *Biochemical models of leaf Photosynthesis*. (CSIRO Publishing, 2000).
- 37 Xu, F. *et al.* Overexpression of rice aquaporin OsPIP1;2 improves yield by enhancing mesophyll CO₂ conductance and phloem sucrose transport. *Journal of Experimental Botany* **70**, 671-681, doi:10.1093/jxb/ery386 (2019).
- 38 McGaughey, S. A., Qiu, J., Tyerman, S. D. & Byrt, C. S. in *Annual Plant Reviews online* 381-416 (2018).
- 39 Gambetta, G. A., Knipfer, T., Fricke, W. & McElrone, A. J. in *Plant aquaporins* 133-153 (Springer, 2017).
- 40 Stemmet, M. C., De Bruyn, J. A. & Zeeman, P. B. THE UPTAKE OF CARBON DIOXIDE BY PLANT ROOTS. *Plant and Soil* **17**, 357-364 (1962).
- 41 Hibberd, J. M. & Quick, W. P. Characteristics of C₄ photosynthesis in stems and petioles of C₃ flowering plants. *Nature* **415**, 451-454 (2002).

- 42 Mukhopadhyay, R., Bhattacharjee, H. & Rosen, B. P. Aquaglyceroporins: generalized metalloid channels. *Biochimica et biophysica acta* **1840**, 1583-1591, doi:10.1016/j.bbagen.2013.11.021 (2014).
- 43 Ogée, J., Wingate, L. & Genty, B. Estimating mesophyll conductance from measurements of C¹⁸O discrimination and carbonic anhydrase activity. *Plant Physiology* **178**, 728-752, doi:10.1104/pp.17.01031 (2018).
- 44 Pfeffer, M. & Peisker, M. in *Photosynthesis: from light to biosphere* Vol. V (ed P. Mathis) 547-550 (Kluwer Academic Publishers, 1995).
- 45 Nakagawa, S., Niimura, Y., Gojobori, T., Tanaka, H. & Miura, K.-i. Diversity of preferred nucleotide sequences around the translation initiation codon in eukaryote genomes. *Nucleic acids research* **36**, 861-871, doi:10.1093/nar/gkm1102 (2008).
- 46 Suga, S. & Maeshima, M. Water Channel Activity of Radish Plasma Membrane Aquaporins Heterologously Expressed in Yeast and Their Modification by Site-Directed Mutagenesis. *Plant and Cell Physiology* **45**, 823-830, doi:10.1093/pcp/pch120 (2004).
- 47 Endeward, V. *et al.* Evidence that aquaporin 1 is a major pathway for CO₂ transport across the human erythrocyte membrane. *The FASEB Journal* **20**, 1974-1981, doi:<https://doi.org/10.1096/fj.04-3300com> (2006).
- 48 Bertl, A. & Kaldenhoff, R. Function of a separate NH₃-pore in Aquaporin TIP2;2 from wheat. *FEBS Letters* **581**, 5413-5417, doi:<https://doi.org/10.1016/j.febslet.2007.10.034> (2007).
- 49 Otto, B. *et al.* Aquaporin Tetramer Composition Modifies the Function of Tobacco Aquaporins. *Journal of Biological Chemistry* **285**, 31253-31260 (2010).
- 50 Yang, B. *et al.* Carbon Dioxide Permeability of Aquaporin-1 Measured in Erythrocytes and Lung of Aquaporin-1 Null Mice and in Reconstituted Proteoliposomes. *Journal of Biological Chemistry* **275**, 2686-2692 (2000).
- 51 Qiu, J., McGaughey, S. A., Groszmann, M., Tyerman, S. D. & Byrt, C. S. Phosphorylation influences water and ion channel function of AtPIP2;1. *Plant, Cell & Environment* **43**, 2428-2442, doi:<https://doi.org/10.1111/pce.13851> (2020).
- 52 Engler, C. *et al.* A Golden Gate Modular Cloning Toolbox for Plants. *ACS Synthetic Biology* **3**, 839-843, doi:10.1021/sb4001504 (2014).
- 53 Hopp, T. P. *et al.* A Short Polypeptide Marker Sequence Useful for Recombinant Protein Identification and Purification. *Bio/Technology* **6**, 1204-1210, doi:10.1038/nbt1088-1204 (1988).
- 54 Porra, R. J., Thompson, W. A. & Kriedemann, P. E. Determination of accurate extinction coefficients and simultaneous equations for assaying chlorophylls a and b extracted with four different solvents: verification of the concentration of chlorophyll standards by atomic absorption spectroscopy. *Biochimica et Biophysica Acta (BBA) - Bioenergetics* **975**, 384-394, doi:[https://doi.org/10.1016/S0005-2728\(89\)80347-0](https://doi.org/10.1016/S0005-2728(89)80347-0) (1989).
- 55 Pengelly, J. J. L. *et al.* Growth of the C₄ dicot *Flaveria bidentis*: photosynthetic acclimation to low light through shifts in leaf anatomy and biochemistry. *Journal of Experimental Botany* **61**, 4109-4122 (2010).
- 56 von Caemmerer, S. *et al.* Carbonic anhydrase and C₄ photosynthesis: a transgenic analysis. *Plant Cell Environ* **27**, 697-703 (2004).
- 57 Jenkins, C. L., Furbank, R. T. & Hatch, M. D. Mechanism of c(4) photosynthesis: a model describing the inorganic carbon pool in bundle sheath cells. *Plant physiology* **91**, 1372-1381 (1989).
- 58 Ruuska, S. A., Andrews, T. J., Badger, M. R., Price, G. D. & von Caemmerer, S. The role of chloroplast electron transport and metabolites in modulating Rubisco activity in tobacco. Insights from transgenic plants with reduced amounts of cytochrome b/f complex or glyceraldehyde 3-phosphate dehydrogenase. *Plant physiology* **122**, 491-504 (2000).
- 59 Massey, B. *Understanding betalain regulation in floral and vegetative tissues of Ptilotus cultivars*, The University of Queensland, (2012).
- 60 Martin-Avila, E. *et al.* Modifying Plant Photosynthesis and Growth via Simultaneous Chloroplast Transformation of Rubisco Large and Small Subunits. *The Plant Cell* **32**, 2898, doi:10.1105/tpc.20.00288 (2020).
- 61 Ludwig, M., von Caemmerer, S., Dean Price, G., Badger, M. R. & Furbank, R. T. Expression of Tobacco Carbonic Anhydrase in the C₄ Dicot *Flaveria bidentis* Leads to Increased Leakiness of the Bundle Sheath

and a Defective CO₂-Concentrating Mechanism. *Plant Physiology* **117**, 1071, doi:10.1104/pp.117.3.1071 (1998).

62 Ermakova, M. *et al.* Installation of C4 photosynthetic pathway enzymes in rice using a single construct. *Plant Biotechnology Journal* doi.org/10.1111/pbi.13487, doi:<https://doi.org/10.1111/pbi.13487> (2020).

63 Schindelin, J. *et al.* Fiji: an open-source platform for biological-image analysis. *Nature Methods* **9**, 676-682, doi:10.1038/nmeth.2019 (2012).

64 Genty, B., Briantais, J.-M. & Baker, N. The relationship between the quantum yield of photosynthetic electron transport and and quenching of chlorophyll fluorescence. *Biochimica and Biophysica Acta* **990**, 87-92 (1989).

65 von Caemmerer, S. Updating the steady state model of C₄ photosynthesis. *bioRxiv*, 2021.2003.2013.435281, doi:10.1101/2021.03.13.435281 (2021).

66 DiMario, R. J. & Cousins, A. B. A single serine to alanine substitution decreases bicarbonate affinity of phosphoenolpyruvate carboxylase in C4 *Flaveria trinervia*. *Journal of Experimental Botany* **70**, 995-1004, doi:10.1093/jxb/ery403 (2019).

Table 1. Properties of *S. viridis* plants expressing *SiPIP2;7-FLAG* in mesophyll cells. PEPC, PEP carboxylase; Rubisco, ribulose biphosphate carboxylase oxygenase; LMA, leaf mass per area. Azygous plants of line 44 were used as control. Mean \pm SE, $n = 3$ except for biomass ($n = 8$). Three-weeks old plants before flowering were used for all analyses. No significant difference was found between the transgenic and control plants (One-way ANOVA, $\alpha = 0.05$).

Parameter	Control	Line 27	Line 44	Line 52
PEPC activity, $\mu\text{mol CO}_2 \text{ m}^{-2} \text{ s}^{-1}$	220.1 \pm 25.8	197.6 \pm 12.7	208.7 \pm 7.9	218.5 \pm 3.5
CA hydration rate, $\text{mol m}^{-2} \text{ s}^{-1} \text{ bar}^{-1}$	6.50 \pm 0.10	6.32 \pm 0.22	5.34 \pm 0.67	5.35 \pm 0.56
Rubisco active sites, $\mu\text{mol m}^{-2}$	12.17 \pm 0.63	12.53 \pm 0.54	12.84 \pm 0.13	12.63 \pm 0.74
Chlorophyll ($a+b$), mmol m^{-2}	0.71 \pm 0.07	0.72 \pm 0.04	0.72 \pm 0.05	0.72 \pm 0.08
Chlorophyll a/b	5.01 \pm 0.16	5.08 \pm 0.05	4.97 \pm 0.09	5.07 \pm 0.15
LMA, g (dry weight) m^{-2}	23.6 \pm 1.6	24.0 \pm 1.5	25.6 \pm 1.3	25.4 \pm 1.3
Shoot biomass, g (dry weight) plant^{-1}	2.06 \pm 0.36	2.01 \pm 0.20	2.23 \pm 0.31	2.24 \pm 0.34
Root biomass, g (dry weight) plant^{-1}	0.27 \pm 0.07	0.28 \pm 0.03	0.34 \pm 0.06	0.35 \pm 0.05

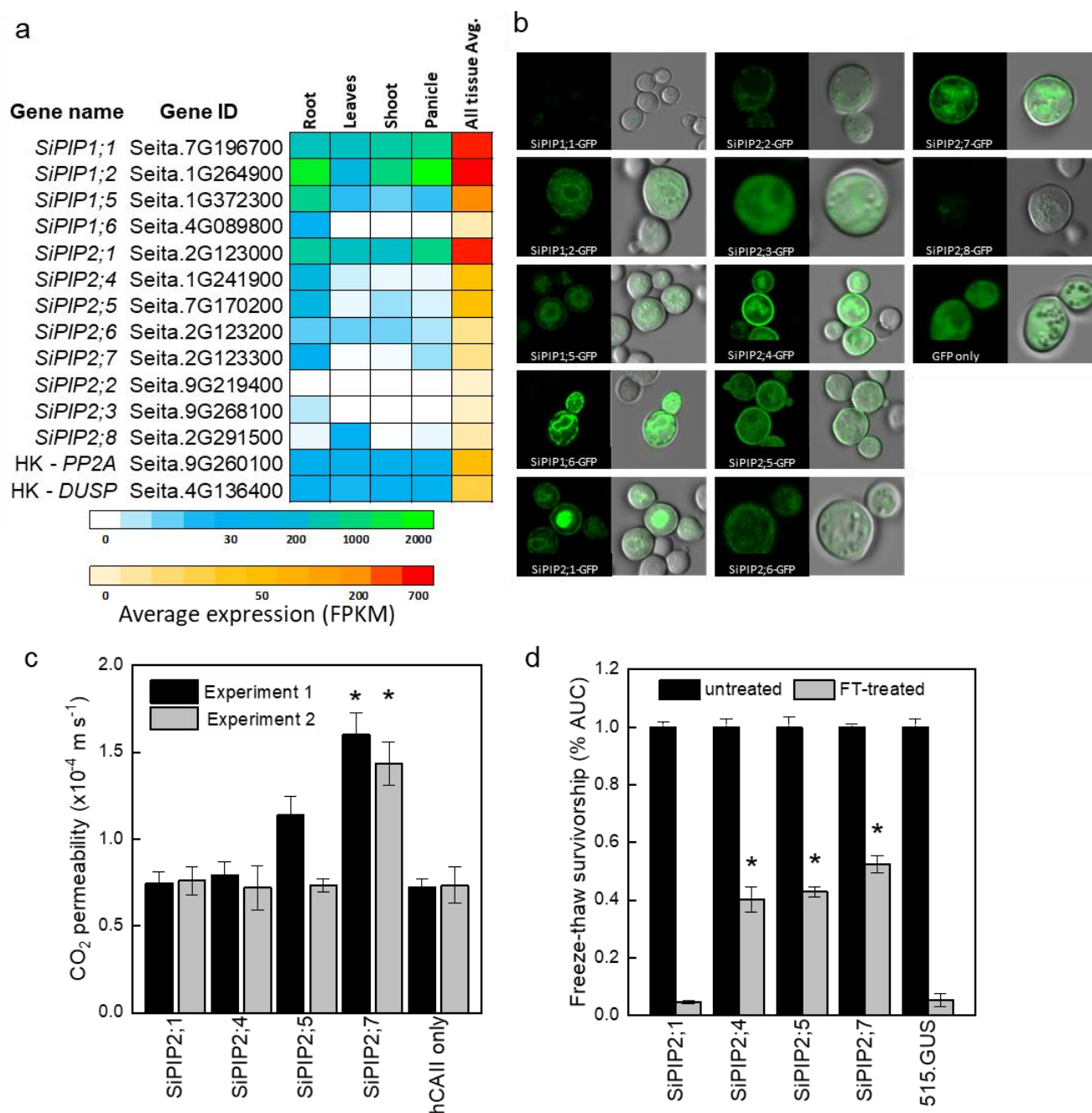


Fig. 1. Identification of the CO₂-permeable aquaporin *SiPIP2;7* from *S. italica*. **a.** Expression atlas of the *SiPIP* genes generated from Phytomine reported as Fragments Per Kilobase of transcript per Million mapped reads (FPKM). House-keeping genes (HK) *PROTEIN PHOSPHATASE 2A* (*PP2A*) and *DUAL SPECIFICITY PROTEIN* (*DUSP*) were included for reference. **b.** Localization of *SiPIP*-GFP fusions expressed in yeast visualised with confocal microscopy; left panels – GFP fluorescence; right panels – bright field overlaid with GFP fluorescence. Measured cell diameters are shown on Fig. S2. **c.** CO₂ permeability assay on yeast co-expressing *SiPIPs* and human *CARBONIC ANHYDRASE II* (*hCAII*) analyzed by stopped flow spectrometry (see Fig. S2 for details). “*hCAII* only” expression was used as negative control. Mean \pm SE, $n = 3$ biological replicates. Two independent experiments are presented. Asterisks

537 indicate statistically significant differences between yeast expressing *SiPIPs* and “hCAII only” control (*t*-
538 test, $P < 0.05$). **d.** Yeast water permeability assessed in the yeast aquaporin deletion background (*aqy1*
539 *aqy2*) by the cumulative growth between untreated and freeze-thawed cells and determined by the
540 percent area under the curve (% AUC). The yeast expressing the β -glucuronidase reporter gene
541 (515.GUS) was used as negative control. Mean \pm SE, $n = 4$ biological replicates. Asterisks indicate
542 statistically significant differences between yeast expressing *SiPIPs* and 515.GUS control (*t*-test, $P <$
543 0.01).

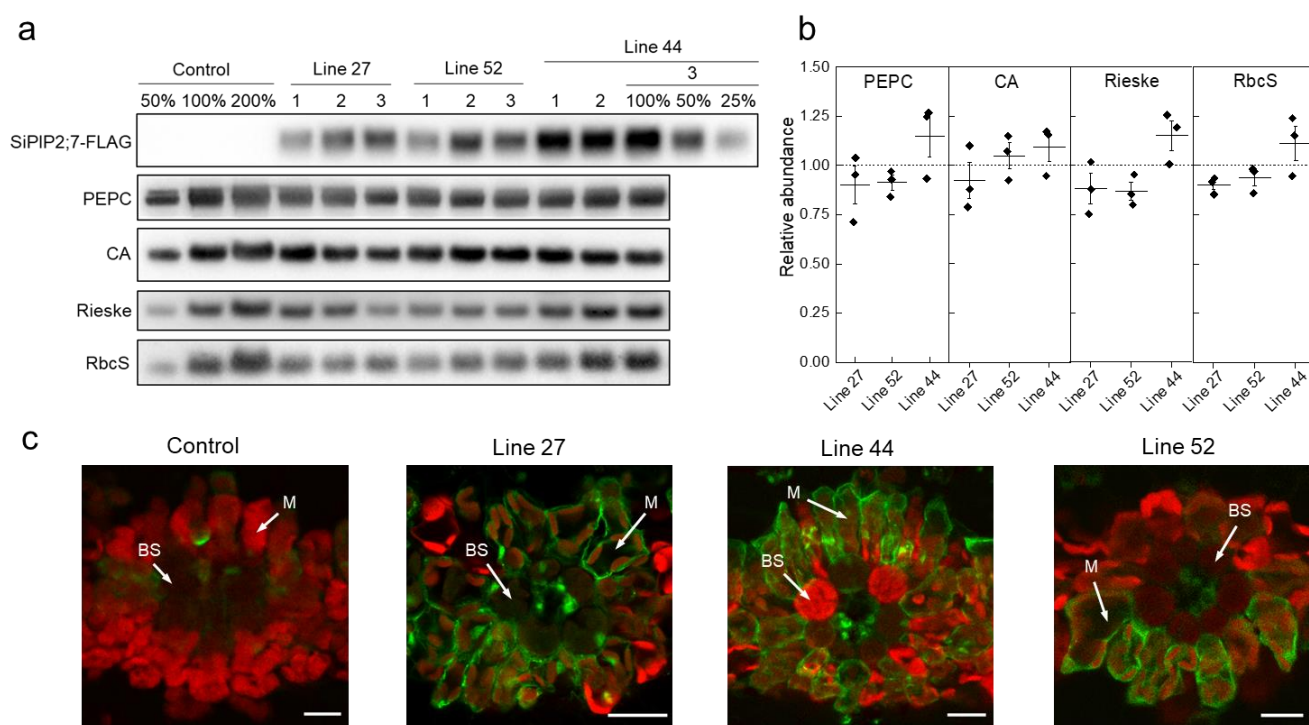


Fig. 2. Characterization of *S. viridis* plants expressing *SiPIP2;7-FLAG* in mesophyll cells. **a.** Immunodetection of SiPIP2;7-FLAG and photosynthetic proteins in leaf protein samples loaded on leaf area basis. Three plants from each of the three transgenic lines were analyzed and dilution series of the control and line 44-3 samples were used for relative quantification. **b.** Protein abundances calculated from the immunoblots relative to control plants. Mean \pm SE. No significant difference was found between the transgenic and control plants (t -test, $P < 0.05$). **c.** Immunolocalisation of SiPIP2;7-FLAG on leaf cross-sections visualized with confocal microscopy. Fluorescence signals are pseudo-colored: green - FLAG antibodies labelled with secondary antibodies conjugated with Alexa Fluor 488; red - chlorophyll autofluorescence. BS, bundle sheath cell; M, mesophyll cell. Scale bars = 20 μ m. Azygous plants of line 44 were used as control.

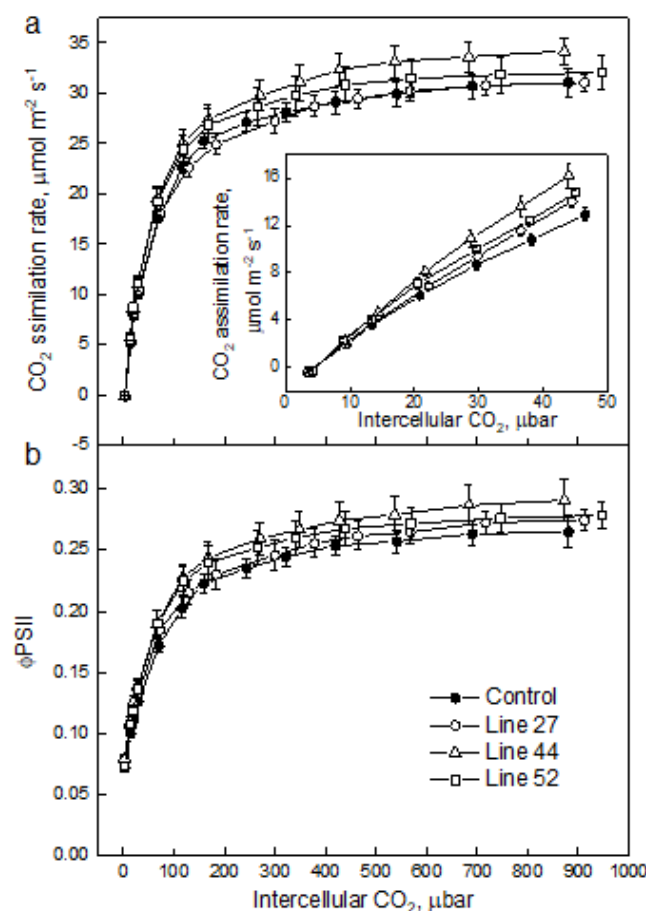


Fig. 3. CO₂ response of CO₂ assimilation rate (a) and quantum yield of Photosystem II (b) in *S. viridis* plants expressing *SiPIP2;7-FLAG* in mesophyll cells. Measurements were performed at the irradiance of 1500 μmol m⁻² s⁻¹; azygous plants of line 44 were used as control. Mean ± SE, *n* = 4-5 biological replicates. No significant difference was found between the transgenic and control plants (One-way ANOVA, α = 0.05).

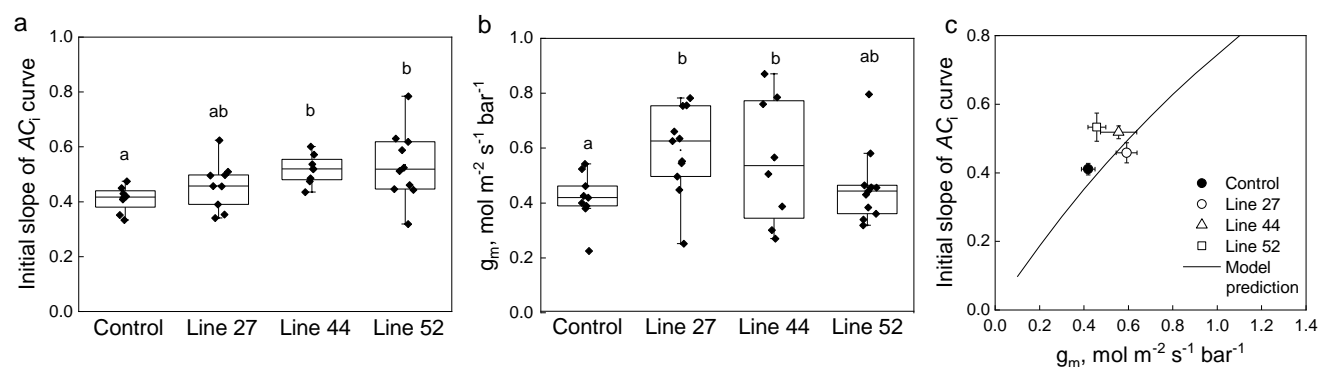


Fig. 4. Effect of the mesophyll conductance, g_m , on the initial slope of the CO_2 assimilation response curve to the intercellular CO_2 partial pressure (AC_i curve) in leaves of *S. viridis* expressing *SiPIP2;7-FLAG* in mesophyll cells. **a.** Mesophyll conductance, g_m , estimated by oxygen isotope discrimination assuming full isotopic equilibrium²³. Measurements were made at ambient CO_2 and low O_2 . **b.** Initial slope of the AC_i curves estimated by linear fitting of curves presented in Fig. 3a inset. **c.** Data from a and b compared to the C_4 biochemical model predictions³⁶. The model relates the initial slope of the AC_i curve (dA/C_i) to g_m by: $\frac{dA}{dC_i} = g_m V_{pmax} / (g_m K_p + V_{pmax})$, where V_{pmax} and K_p denote the maximum PEPC activity and the Michaelis Menten constant for CO_2 taken here as 250 $\mu\text{mol m}^{-2} \text{s}^{-1}$ and 82 μbar ^{65,66}. Azygous plants of line 44 were used as control. Letters indicate statistically significant differences between the groups (One-way ANOVA with Tukey post-hoc test, $\alpha = 0.05$).